Coda Wave Analysis to Monitor Processes in Soils

Sheng Dai, S.M.ASCE[1]; Frank Wuttke[2]; and J. Carlos Santamarina, M.ASCE[3]

Abstract: Small-strain elastic wave propagation is a constant-fabric phenomenon ideally suited to monitor processes in soils. However, the determination of very small changes in travel time limits our ability to resolve changes in soil stiffness caused by internal processes or changes in boundary conditions. The first-arrival reflects the fastest path between the source and receiver of the propagating wave field; later arrivals in the coda correspond to longer paths after multiple boundary reflections and internal scattering. Therefore, time shifts between the codas of two consecutive signals are longer and easier to detect than between the signals' first arrivals. Slight changes in coda waves can be determined by cross-correlating time windows, time-stretched signals, or frequency-stretched spectra. Basic coda analysis assumes a homogeneous velocity change throughout the medium, propagation modes (P, S) that are equally affected by the process and the preservation of V_P/V_S ratio during the process. The resolving power of coda wave interferometry is explored in an experimental study conducted with quartzitic sand subjected to loading, creep, and unloading stages. The results reveal that coda wave analysis can be used to detect changes in wave velocity on the order of $\Delta V/V < 0.1\%$ (this corresponds to a stress change smaller than $\Delta\sigma'/\sigma' \approx 1\%$ in uncemented soils). Such a high velocity resolution permits the study of creep, aging, and diagenetic processes even in relatively short duration tests. **DOI:** 10.1061/(ASCE)GT.1943-5606.0000872.

CE Database subject headings: Sand (soil type); Stiffness; Creep; Wave propagation.

Author keywords: Coda wave interferometry; Cross correlation; Ottawa sand; Stiffness-stress response; Creep; Aging.

Introduction

The characterization of natural soils is inherently challenging due to their particulate nature and the effect of the measurement process on measured properties. Small-strain measurements using elastic waves provide valuable soil information without altering the soil fabric; examples include small-strain stiffness and attenuation, spatial variability, and soil changes during internal or boundary-imposed processes.

A salient problem in wave measurements is the determination of the first arrival in wave fields. Recommended criteria vary for different experimental configurations (examples for bender element tests can be found in Lee and Santamarina 2005; Arroyo et al. 2006; Youn et al. 2008). Furthermore, changes in first arrivals can often fall below detection limits when monitoring phenomena such as diagenesis, creep, and aging.

On the other hand, the signal tail or coda captures multiple scattered and reflected waves that arrive after the fastest wavefront (Aki 1969; Aki and Chouet 1975; Snieder 2006). These later wavefronts have traveled longer paths and accumulated larger time shifts. Therefore, coda analysis or coda wave interferometry may provide process information even when changes in first arrivals are below resolution. Coda wave analysis has been used to evaluate slight changes in fields, such as earthquake engineering, volcano monitoring, fault movement, and material characterization (Snieder et al. 2002; Gret 2004; Shapiro et al. 2005; Snieder 2006; Otheim et al. 2011; Schurr et al. 2011; Wuttke et al. 2012).

This study identifies and compares algorithms for basic coda wave analysis, highlights underlying assumptions in coda interpretation, and demonstrates the methodology using experimental data gathered to assess the stiffness evolution of a uniform quartzitic sand specimen during loading, creep, and unloading processes. Eventually, the enhanced signal processing methodology provides new insight into soil behavior.

Analysis of Seismic Codas

The concept of coda wave analysis is introduced herein. For clarity, the sampling interval Δt is the time separation between two contiguous discrete values in a digital signal, and a time window is a signal segment between two predefined times.

Consider two consecutive P wave signals A and B obtained for a sandy specimen under isotropic confinement, the first one at 67.6 kPa (9.8 psi) and the second one at 68.9 kPa (10 psi), as shown in Fig. 1(a). The time for the first arrival t_D is identical in both signals ($t_D \approx 200$ μs), yet time windows taken in the range of 1,800–2,200 μs (i.e., 9–11 times the travel time for the first arrival t_D) and 3,600–4,000 μs (i.e., 18–20 times t_D) show that coda waves accumulate time shifts.

The time delay for a given event in the two signals increases linearly with travel distance l, that is, with the event time $t = l/V$, as shown in Fig. 1(b). The slope of the trend in Fig. 1(b) is $\theta = \Delta t/t$. For a velocity change from V_A to $V_B = V_A + \Delta V$

$$\theta = \frac{\Delta t}{t_A} = \frac{t_A - t_B}{t_A} = \frac{\frac{l}{V_A} - \frac{l}{V_B}}{\frac{l}{V_A}} = \frac{V_B - V_A}{V_B} \cong \frac{\Delta V}{\overline{V}} \tag{1}$$

where the average velocity is $\overline{V} = (V_A + V_B)/2$. Eq. (1) shows that the slope of time lags θ is equal to the relative change in velocity $\Delta V/\overline{V}$ between signals A and B.

[1]Ph.D. Candidate, School of Civil and Environmental Engineering, Georgia Institute of Technology, 790 Atlantic Drive, Atlanta, GA 30332-0355 (corresponding author). E-mail: sheng.dai@gatech.edu

[2]Professor, Geomechanics, Civil Engineering, Bauhaus-Universität Weimar, 99423 Weimar, Germany. E-mail: frank.wuttke@uni-weimar.de

[3]Professor, School of Civil and Environmental Engineering, Georgia Institute of Technology, Atlanta, GA 30332-0355. E-mail: jcs@gatech.edu

Note. This manuscript was submitted on January 30, 2012; approved on November 26, 2012; published online on November 28, 2012. Discussion period open until February 1, 2014; separate discussions must be submitted for individual papers. This paper is part of the ***Journal of Geotechnical and Geoenvironmental Engineering***, Vol. 139, No. 9, September 1, 2013. ©ASCE, ISSN 1090-0241/2013/9-1504–1511/$25.00.

J. Geotech. Geoenviron. Eng. 2013.139:1504-1511.

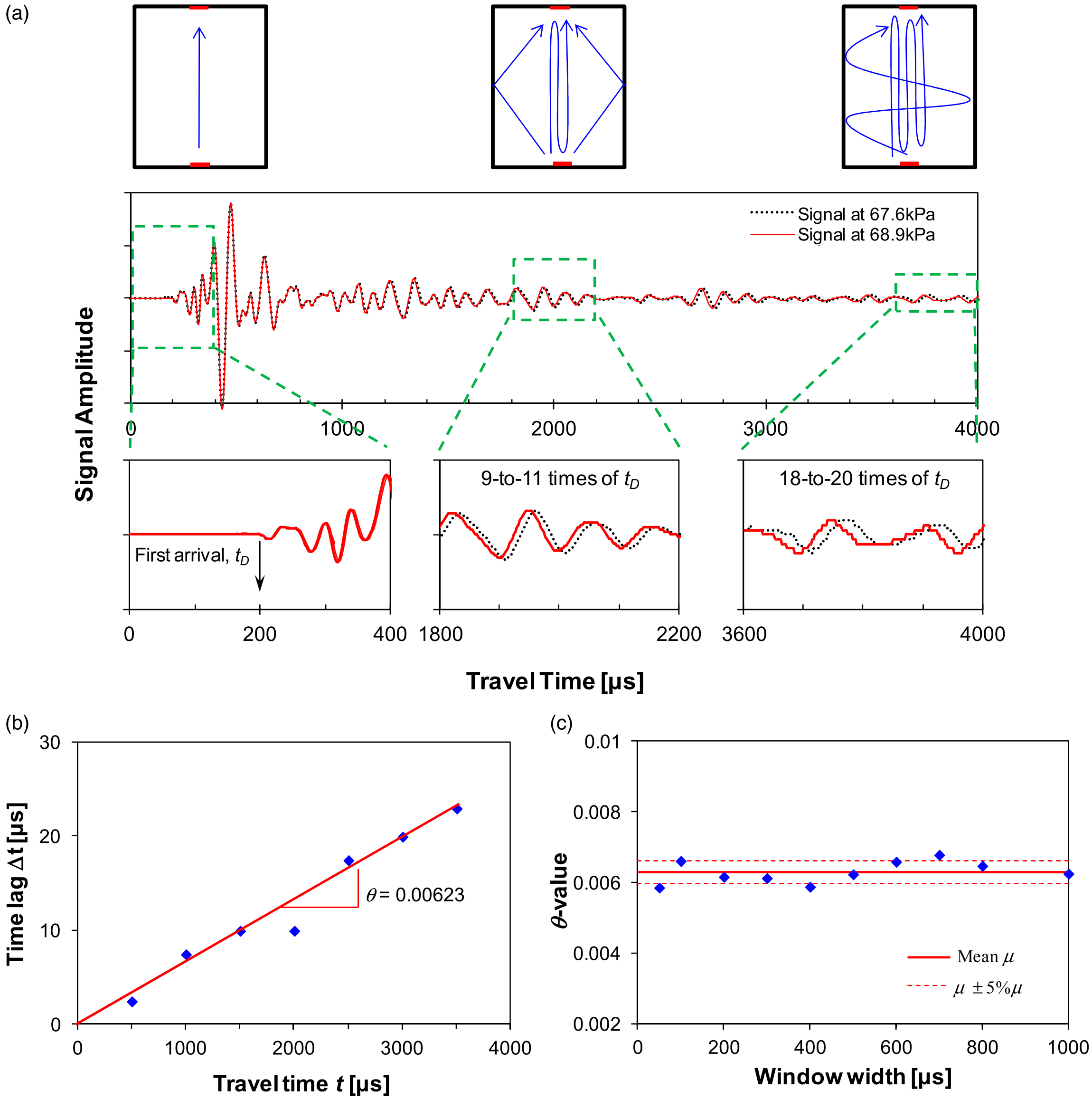

Fig. 1. Schematic illustration of seismic coda analysis; (a) the first arrival of a wave signature reflects the fastest wave pathway (Fermat's principle); events that have experienced multiple reflections arrive later in the coda. Therefore, codas accumulate differences in propagation velocity; (b) time lag Δt between two signals increases almost linearly with propagation time t; the slope θ is the stretching factor; (c) the value of θ varies slightly with window width in time-windowed cross correlations; differences in θ values attributable to the window width are mostly within 5%

It follows from Eq. (1) that a certain event at time t_A in signal A appears at a stretched time $t_B = t_A(1+\theta)$ in signal B. Thus, the slope θ is herein referred to as the stretching factor. Three different methods to determine the stretching factor θ are presented next.

Method 1: Short-Time Cross Correlation

Short-time windows are extracted from the full signals A and B, and the relative time lag Δt between the windowed signals is determined by cross correlation (Snieder et al. 2002; Santamarina and Fratta 2005; Wuttke et al. 2012). Multiple time lags are obtained by repeating time windowing and cross correlation at different positions along the signals. The time lag Δt determined for each window position is plotted versus the window central time t_W to determine θ, as shown in Fig. 1(b). Window width and superposition must be selected a priori. Computed θ values vary slightly with window width, as shown in Fig. 1(c).

Method 2: Time-Stretched Cross Correlation

The linear increase in time lag Δt with travel time t for corresponding events in signals A and B implies that waveforms can overlap by linearly stretching the timescale of the faster one, say signal B (Sens-Schönfelder and Wegler 2006). The procedure consists of four steps: (1) select a value for θ; (2) time-stretch the faster signal B using $t_B = t_A(1+\theta)$; (3) compute the cross correlation between the full-length signals, that is, the original signal A and the stretched signal B; (4) repeat steps 1 through 3 for other θ values. The sought value of θ is the one that renders the highest cross correlation, as shown in Fig. 2(a). Note that time-stretching requires resampling: new signal values at all times t_i are obtained by interpolating between stretched signal values that fall immediately above and below t_i (we use linear interpolation).

Signal amplitudes decrease with time; thus, cross correlation values are biased by the earlier higher energy events in the signals.

J. Geotech. Geoenviron. Eng. 2013.139:1504-1511.

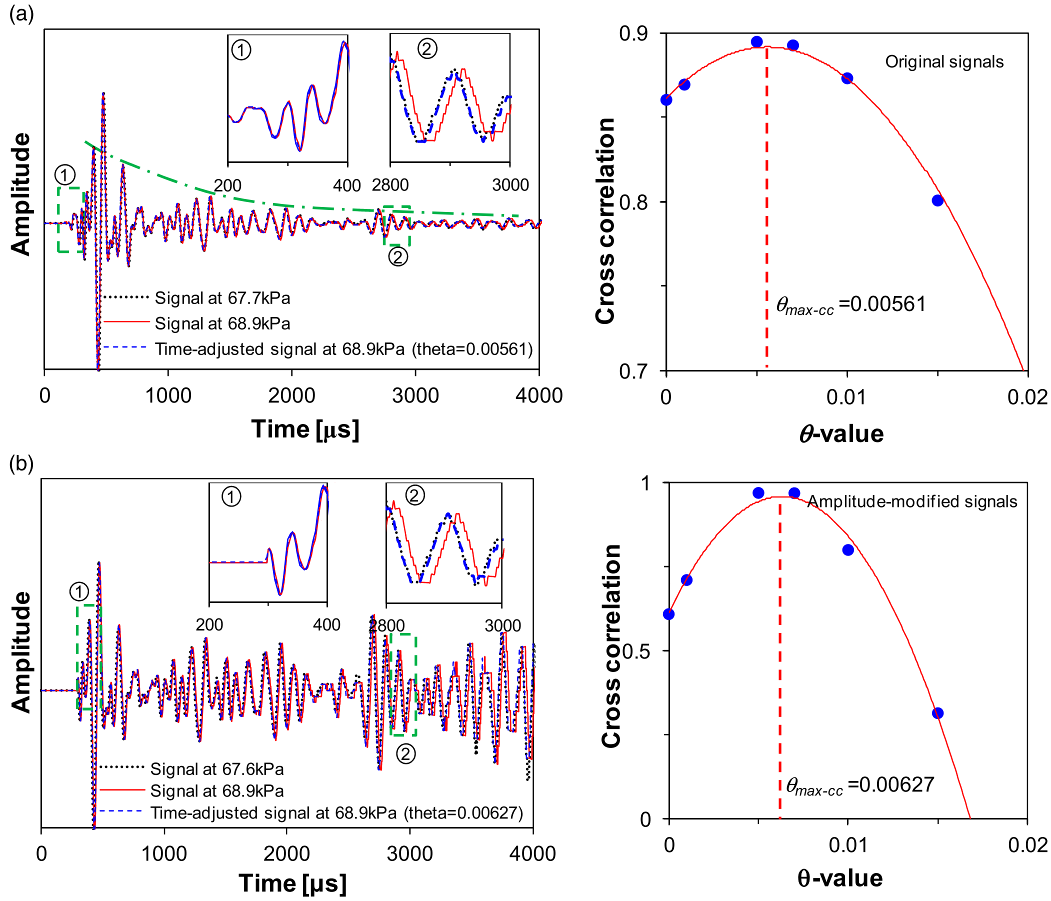

Fig. 2. Time-stretched cross correlation: full-signal based determination of the stretching factor θ in the time domain; (a) computations using original signals; (b) both signals are exponentially amplified [dashed-dotted line in (a)] to obtain constant energy content in time before computing the cross correlation: the signal value x_i at time t_i is amplified by a factor $e^{\alpha t i}$ where α is constant for all t_i and equal for both signals; inserts show amplified signal windows (denoted as 1 and 2)

This bias is overcome by premultiplying both signals A and B by the same exponential amplifier, as shown by the dashed-dotted line in Fig. 2(a), to yield signals with constant energy content in time, as shown in Fig. 2(b): the signal value x_i at time t_i is amplified by a factor $e^{\alpha t i}$, where α is constant for all t_i and equal for both signals.

Method 3: Frequency-Stretched Spectra

Two signals A and B with a linear increase in time lag can be regarded as the same signal but sampled with two different sampling intervals: signal A using Δt, and signal B with $(1 \pm \theta)\Delta t$. In other words, their amplitudes are identical when the discrete time $t_A = i \times \Delta t$ equals $t_B = i \times [(1 \pm \theta)\Delta t]$, where i is an integer. Therefore, in the frequency domain, the spectral magnitude for signal A at frequency $\omega_A = 2\pi u/(N \times \Delta t)$ equals that for signal B at $\omega_B = 2\pi u/[N \times (1 \pm \theta)\Delta t]$, where the integer u is the frequency counter and N is the number of discrete points in the sampled signal. Then, the stretching coefficient can be determined in the frequency domain as follows: (1) compute the frequency spectrum for both signals A and B; (2) linearly stretch the spectrum of the slower signal until both spectra match best (i.e., cross correlation—note that this requires interpolation to compute stretched spectral values at frequencies ω_u); (3) the sought value of θ is the one that corresponds to the best match between the two spectra. The results are shown in Fig. 3 for the same signal pair used earlier.

Comparison

The values in Figs. 1, 2, and 3 were obtained for the same signal pair. The computed stretching factors are (a) short-time cross correlation $\theta = 0.00623$ ($\pm 5\%$ for different window widths), (b) amplitude-adjusted time-stretched cross correlation $\theta = 0.00627$; and (c) cross correlation of the frequency-stretched spectra $\theta = 0.00628$. From Eq. (1), the stretching factor is $\theta = \Delta V/V$, hence, θ-values measured in this example indicate that a 0.6% velocity change has taken place in the medium between signals A and B (i.e., a 1.4 kPa isotropic stress increase).

Experimental Study: P Wave Velocity in Dry Sand

The purpose of this experimental study is to explore the potential of coda wave analysis in detecting very small velocity changes. We study two cases: velocity changes due to small changes in effective stress, and the more challenging case of velocity changes during creep aging.

Experiment Design

Specimen

A cylindrical soil specimen (radius $R = 17.5$ mm and height $H = 74.4$ mm) is confined by a latex membrane and subjected to isotropic stress in a triaxial chamber (Fig. 4). The soil selected for this study is Ottawa-20/30 sand (quartzitic; median grain size $d_{50} = 0.72$ mm;

J. Geotech. Geoenviron. Eng. 2013.139:1504-1511.

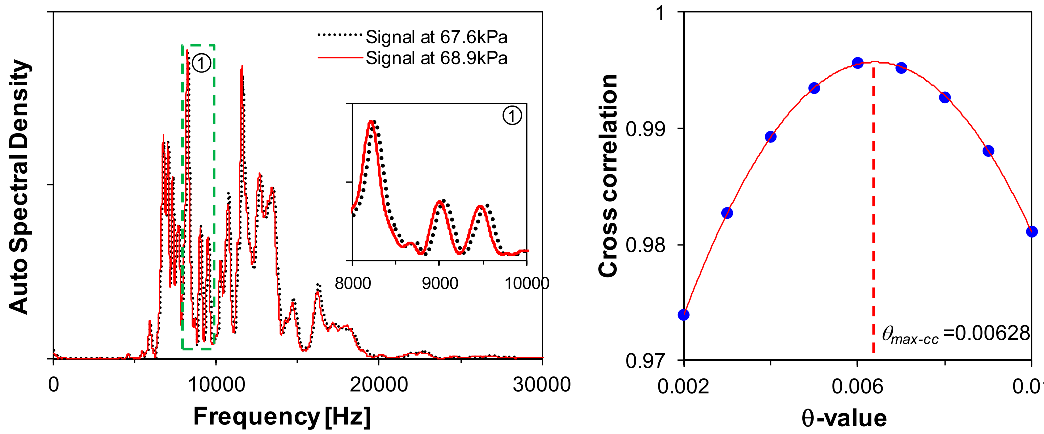

Fig. 3. Stretched spectra: full-signal-based determination of the stretching factor θ in the frequency domain

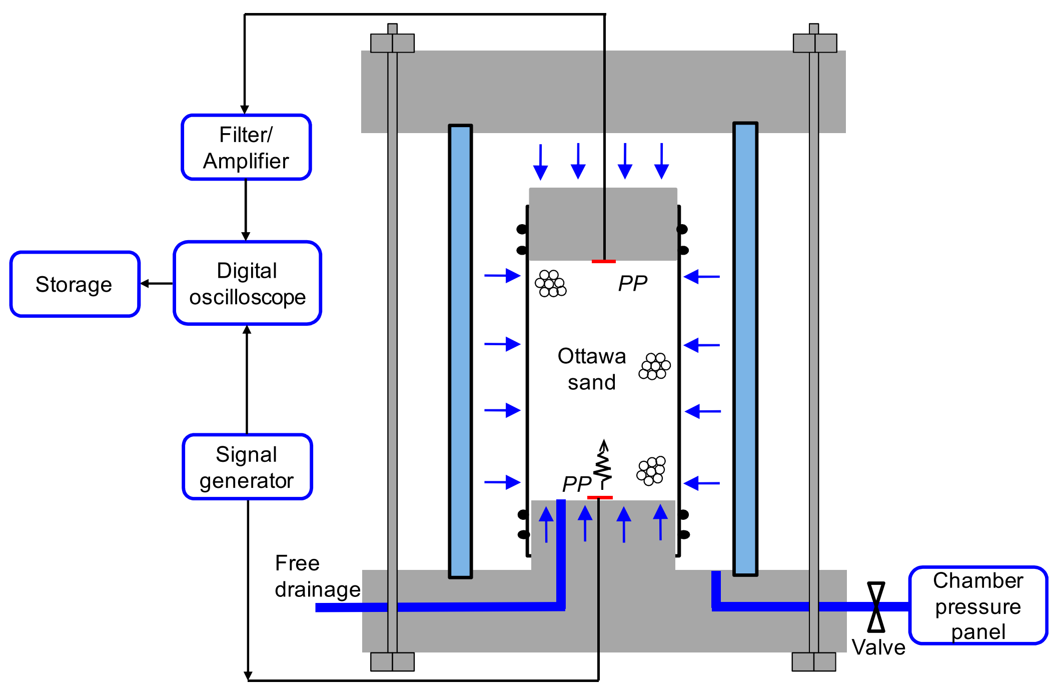

Fig. 4. Experimental configuration; stiffness evolution in uniform quartzitic dry sand subjected to isotropic gas confinement (as illustrated with the arrows); P waves are generated and detected using piezopads (*PP*)

coefficient of uniformity $C_u = 1.2$; roundness $R = 0.9$; sphericity $S = 0.9$; packing $e_{\max/\min} = 0.742/0.502$).

Testing Procedure

The load history involves three stages. (1) Loading: the confining stress is gradually increased from 0 kPa until 68.9 kPa, in 1.4 kPa steps (note that the confining stress is actually measured in PSI and converted into kPa; the loading is increased from 0 to 10 psi, in 0.2 psi steps). (2) Creep: the applied confining stress is held constant at 68.9 kPa for approximately 8 h. (3) Unloading: the confining stress is gradually decreased back to 0 kPa in −1.4 kPa steps.

Wave Propagation

Piezopads are installed on the caps of the sample to monitor the evolution of P wave velocity in the sand. Received wave signals are recorded at each loading step and periodically during creep.

Data Reduction

The reference first arrival travel time is determined for the signal gathered at isotropic confinement $\sigma' = 34.5$ kPa in this study, where the first arrival is very clear. All other travel times are compared to this one through consecutive stretching coefficients $t_B = t_A(1 + \theta)$, as discussed earlier.

Test Results

The complete cascade of 110 signals recorded during loading, creep, and unloading stages is shown in Fig. 5. The horizontal axis shows the wave travel time and the vertical axis shows the waveforms cascading in chronological sequence from the beginning of the test until the end. Signal amplitude is captured with gray intensity: white denotes waveform peaks and black denotes troughs. Travel times shorten during loading and creep. Particularly during creep, differences in first arrival times cannot be visually distinguished (in

J. Geotech. Geoenviron. Eng. 2013.139:1504-1511.

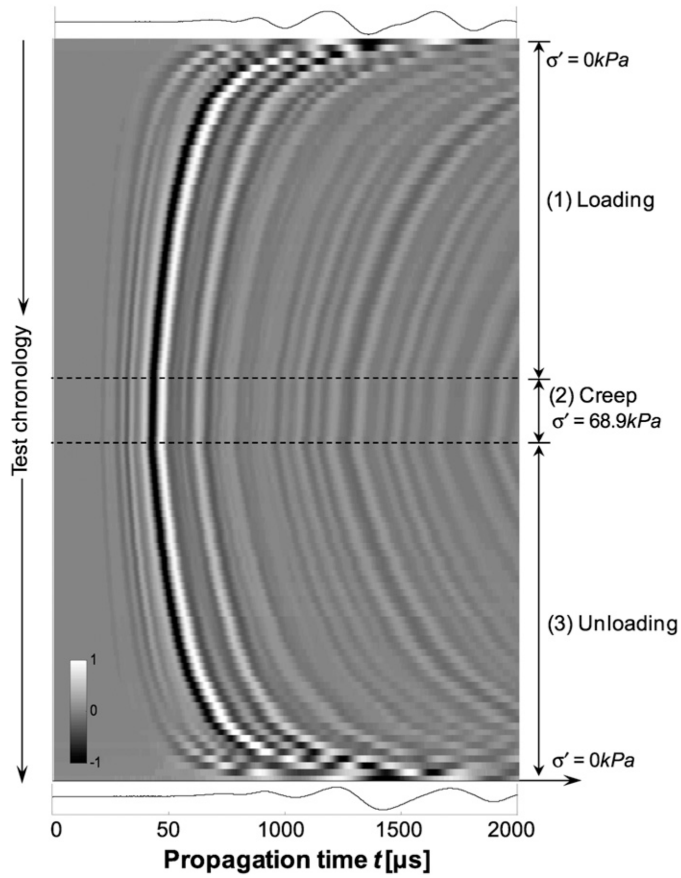

Fig. 5. Cascade of received wave signals (in total 110 waveforms; the first and last signals are shown at the top and bottom of the signal cascade); the signal amplitude is illustrated in gray intensity, where white represents peaks and black troughs; (1) loading from self-weight $\sigma' = 0$ kPa to $\sigma' = 68.9$ kPa in $\Delta\sigma' = 1.4$ kPa (0.2 psi) increments; (2) creep at constant confining pressure ($\sigma' = 68.9$ kPa); (3) unloading from $P = 68.9$ kPa to self-weight in $\Delta\sigma' = -1.4$ kPa drops; note the increasing gradient of peaks and troughs in wave codas recorded during the creep stage

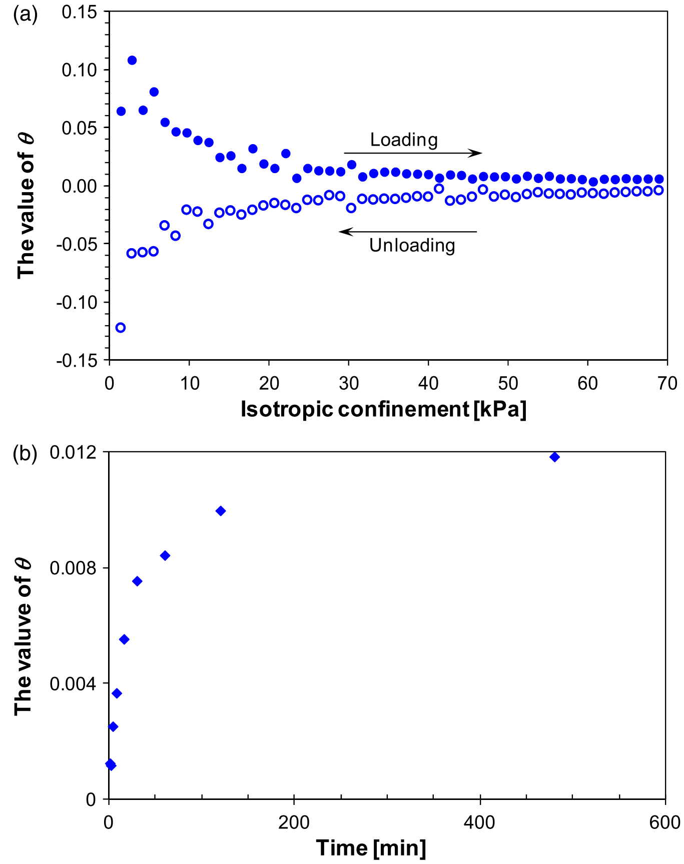

Fig. 6. Computed θ values (a) during loading and unloading; (b) during creep

fact, they may be smaller than the sampling interval $\Delta t = 0.25$ μs). However, codas show clear time shifts of peaks and troughs, even during the creep stage.

Fig. 6 shows computed θ values for all consecutive signals using the short-time cross-correlation method. Computed P wave velocities during the three experimental stages are then presented in Fig. 7(a). The initial P wave velocity of the specimen under self-weight is 110.0 m/s. Velocity increases with confining stress to reach 292.2 m/s at 68.9 kPa, and decreases during unloading to a final value of 119.0 m/s. Fig. 7(b) shows the time-lapse velocity change for the Ottawa sand specimen during creep under constant isotropic confinement $\sigma' = 68.9$ kPa (note that the velocity is plotted in high resolution). The increase in velocity due to creep is $\Delta V_P \approx 1.5\%$ within 8 h of monitoring, and velocity changes as small as $\Delta V/V < 0.1\%$ are detected between consecutive signals.

Analysis

Velocity-Stress Response

Velocity-Stress Power Relationship

A power-type Hertzian relationship adequately captures velocity stress in soils (Santamarina et al. 2001)

$$V = \alpha\left(\frac{\sigma'}{\sigma'_{\mathrm{ref}}}\right)^{\beta} \tag{2}$$

where α is the soil wave velocity when σ' equals the reference effective stress σ'_{ref}, and β reflects the dependency of velocity on effective stress σ' in the direction of wave propagation. Wave velocities measured at $\sigma' > 10$ kPa are well fitted with Eq. (2) ($\alpha = 93.0$ m/s and $\beta = 0.27$ during loading, and $\alpha = 98.0$ m/s and $\beta = 0.26$ during unloading). Stiffness hysteresis in quartzitic sands subjected to isotropic loading is easily missed in standard visual signal interpretation. However, this is clearly seen in the coda-based data plotted in Fig. 7(a). This hysteresis behavior may possibly be due to slight changes in fabric and/or interparticle contact behavior.

Self-Weight Effect

Measured velocities at lower confinement stresses (i.e., $< \sim 10$ kPa in this study) deviate from the velocity-stress power relationship. This is because soil self-weight induces an inhomogeneous stress distribution inside of the specimen that has not been captured in the velocity-stress relationship.

At zero confinement ($\sigma' = 0$), the vertical effective stress in the sediment increases linearly with depth due to self-weight, from $\sigma'_z = \sigma_{\mathrm{cap}}$ (top cap at $z = 0$) to $\sigma'_z = \sigma_{\mathrm{cap}} + \gamma_s H$ at the bottom of the specimen (height H and unit weight γ_s). This stress field must be accounted for during the analysis of P wave velocity data obtained at very low confining stress. Travel time is an integral of slowness $1/V_z$ along the specimen height H

J. Geotech. Geoenviron. Eng. 2013.139:1504-1511.

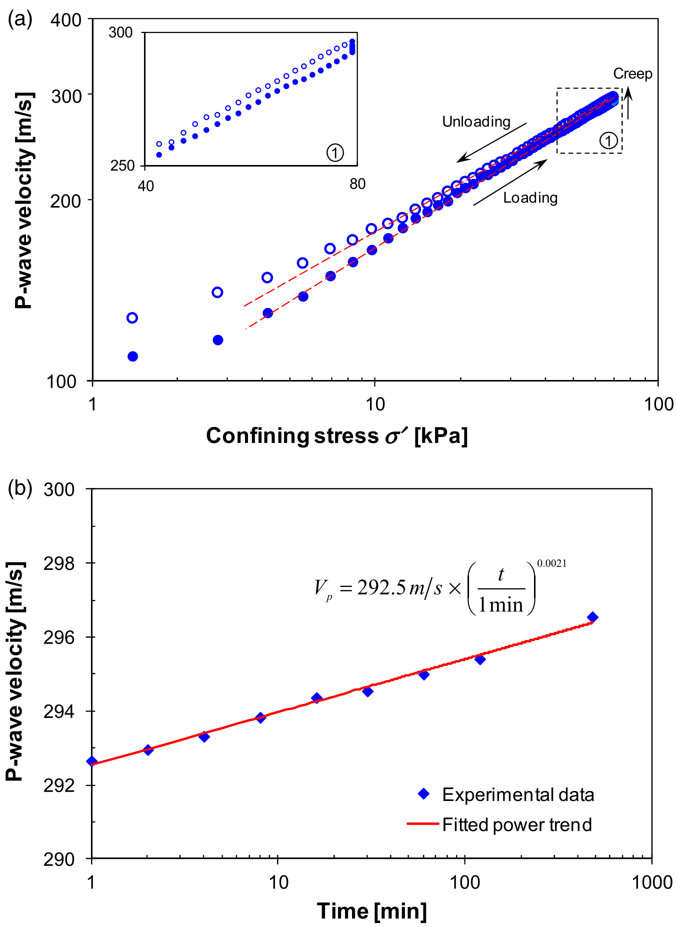

Fig. 7. P wave velocity evolution (a) as a function of applied confining stress σ' during loading (solids) and unloading (circles) stages; the insert amplifies changes in stiffness due to creep during sustained loading $\sigma' = 68.9$ kPa; (b) as a function of time during creep (diamonds) at constant confining stress $\sigma' = 68.9$ kPa

$$t = \int_0^H \frac{dz}{\alpha\left(\frac{\sigma'_z}{\sigma'_{\text{ref}}}\right)^{\beta}} = \int_0^H \frac{dz}{\alpha\left(\frac{\sigma'_0 + \sigma_{\text{cap}} + \gamma_s z}{\sigma'_{\text{ref}}}\right)^{\beta}}$$
$$= \frac{1}{\alpha\gamma_s(1-\beta)}\left[\left(\frac{\sigma'_0 + \sigma_{\text{cap}} + \gamma_s H}{\sigma'_{\text{ref}}}\right)^{1-\beta} - \left(\frac{\sigma'_0 + \sigma_{\text{cap}}}{\sigma'_{\text{ref}}}\right)^{1-\beta}\right] \tag{3}$$

where σ'_0 is the applied isotropic confining stress. Travel times determined using coda analysis are plotted as a function of isotropic confining stress in Fig. 8. We concluded that when self-weight is accounted for at low confining stress, the power velocity-stress relation [Eq. (2)] properly reproduces the complete data set [cf. Figs. 7(a) and 8].

If self-weight is neglected, predicted travel times t_p are much longer than measured times-t_m at low confinement (Fig. 8). For a given sediment with parameters α and β, the ratio t_p/t_m is a function of the ratio between self-weight and confining stress, $\gamma_s H/(\sigma'_0 + \sigma_{\text{cap}})$. From Eq. (3)

$$\frac{t_p}{t_m} = \frac{\frac{\gamma_s H}{\sigma' + \sigma_{\text{cap}}}(1-\beta)}{\left(1 + \frac{\gamma_s H}{\sigma'_0 + \sigma_{cap}}\right)^{1-\beta} - 1} \tag{4}$$

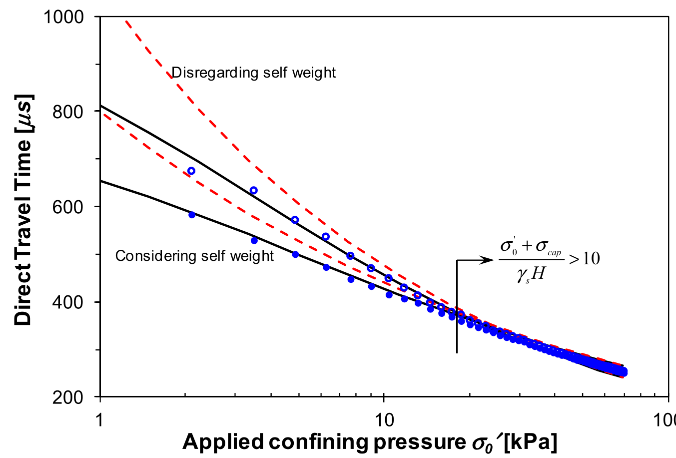

Fig. 8. Predicted (solid lines: considering the self-weight effect; dashed lines: disregarding the self-weight effect) versus measured (dots) direct travel time as a function of applied confining pressure σ'_0; accounting for self-weight requires time integration along the specimen

For $\beta = 0.25$, the error in travel time due to self-weight is less than 1% when $(\sigma'_0 + \sigma_{\text{cap}})/(\gamma_s H) > 10$. In other words, the effect of self-weight on soil stiffness can be negligible when the confining stress is at least 10 times larger.

Velocity-Stress Parameter β and the Stretching Factor θ

The stretching factor θ between two consecutive signals gathered at stresses σ'_A and σ'_B reflects the stress-dependent velocity change. Indeed, combining Eqs. (1) and (2) yields

$$\theta = 1 - \left(\frac{\sigma'_B}{\sigma'_A}\right)^{\beta} \tag{5}$$

This result anticipates the ability of coda waves to resolve changes in mean stress smaller than 1% in uncemented sands (assuming $\theta = 0.001$ and $\beta = 0.25$).

Creep in Dry Sandy Specimen

Computed wave velocities in the sand specimen tested during the creep stage follow a power law with time, as shown in Fig. 7(b)

$$V_P = a\left(\frac{t}{t_{\text{ref}}}\right)^{b} = 292.5\left(\frac{t}{1\ \text{min}}\right)^{0.0021} \tag{6}$$

where the parameter a is the P wave velocity under constant confinement at the reference time t_{ref} (in this case, $t_{\text{ref}} = 1$ min), and the exponent b reflects the rate of creep-dependent stiffening. Both a and b are experimentally determined parameters, and are inherently governed by confining conditions and sediment characteristics.

The creep strain rate $\dot{\varepsilon}$ of a particulate medium at constant effective stress is a function of stress σ' and time t (Singh and Mitchell 1968; Mitchell and Soga 2005)

$$\dot{\varepsilon} = k\left[\frac{\sigma'}{\sigma'_{\text{ref}}}\right]^{m}\left[\frac{t_{\text{ref}}}{t}\right]^{n} \tag{7}$$

where k, m, and n are sediment-dependent parameters, and σ'_{ref} and t_{ref} are the reference stress and time. At the particle level, the tangential normal stiffness E_T in a Hertzian system can be related to the

J. Geotech. Geoenviron. Eng. 2013.139:1504-1511.

axial strain ε_z as (simple cubic packing, Richart et al. 1970; Cascante and Santamarina 1996)

$$E_T = \frac{G_m}{1 - \nu_m} \varepsilon_Z^{1/2} \tag{8}$$

where G_m and ν_m are the shear modulus and Poisson's ratio of the material that makes the grains. The strain at time t is obtained by integrating Eq. (7), and it is replaced in Eq. (8) to obtain a general expression for the evolution of velocity during soil creep as a function of stress σ' and time t

$$V_P = \sqrt{\frac{E}{\rho}} = \sqrt{\frac{G_m}{\rho(1-\nu_m)}} \left(\frac{k t_{\mathrm{ref}}}{1-n}\right)^{\frac{1}{4}} \left(\frac{\sigma'}{\sigma'_{\mathrm{ref}}}\right)^{\frac{m}{4}} \left(\frac{t}{t_{\mathrm{ref}}}\right)^{\frac{1-n}{4}} \tag{9}$$

Most soils have an n value that ranges between 0.75 and 1 (Singh and Mitchell 1968; lower values reported in Singh and Mitchell 1969; Campanella and Vaid 1974). The fitted n value for the quartzitic sand tested in this study is $n = 0.9916$ [cf. Eqs. (6) and (9)], indicating a slow velocity change with time under a confinement of 68.9 kPa.

Discussion: Underlying Assumptions in Coda Analysis

Basic coda analysis presumes that changes in the medium cause identical proportional velocity changes $\Delta V/V$ on all wave paths and propagation modes. In particular, P wave and S wave velocities must be equally affected by the process, that is, V_P/V_S remains constant and θ values for P and S components are identical, θ_P/θ_S. This condition applies to dry or unsaturated soils. In saturated soils, the P wave velocity is primarily controlled by the fluid bulk modulus; thus, only a minor increase in $\Delta V_P/V_{P_0}$ takes place during loading, while the change in $\Delta V_S/V_{S_0}$ can be large.

We highlight that basic coda analysis reveals the relative stretching factor between two waveforms. An absolute wave travel time is required as reference value to determine velocity and velocity changes. Typically, the waveform with the clearest first arrival is selected to determine the reference travel time.

Conclusions

Slight velocity changes in a soil specimen that cause undetectable changes in the first arrival may be measured using coda wave analysis. Values smaller than $\Delta V/V < 0.1\%$ were detected in this study.

The proportional change in velocity is mathematically equal to the stretching factor $\theta = \Delta V/V$. There are robust signal processing algorithms to determine the stretching factor θ between consecutive signals. They involve the cross correlation of either (1) short-time windows, (2) time-stretched signals, or (3) frequency-stretched spectra.

Basic coda wave analysis applies to systems with homogeneous velocity changes and constant V_P/V_S ratio. This is the case in dry and partially saturated soils.

The high velocity resolution attained with coda wave analysis allows for the determination of wave velocities during small stress changes, creep, diagenesis, and aging, where subtle contact-level processes can only be detected by high resolution signal interpretation. Coda wave analysis can resolve a $\Delta\sigma'/\sigma < 1\%$ change in mean effective stress.

Self-weight induces an inhomogeneous stress distribution inside of a specimen. Data reduction must consider gravity effects when the boundary effective stress is less than 10 times the gravity-induced stress.

In agreement with existing creep models, experimental results show that velocity increases during soil creep under constant confinement and follows a power law as a function of time. The exponent can be readily measured using coda wave analysis even when stable quartzitic sands are tested for a relatively short duration.

Acknowledgments

Support for this research was provided by the Chevron-managed DOE/NETL Methane Hydrate Project DE-FC26-01NT41330 and Gulf of Mexico Gas Hydrate Joint Industry Project; R&D Program Geotechnologien funded by the German Research Foundation and German Ministry of Education and Research (Grant 03G0636B), as well as the European Regional Development Fund (Grant FKZB715-09010). Additional funding was provided by the Goiuzeta Foundation.

References

Aki, K. (1969). "Analysis of seismic coda of local earthquakes as scattered waves." *J. Geophys. Res.*, 74(2), 615–631.

Aki, K., and Chouet, L. B. (1975). "Origin of coda waves: Source, attenuation, and scattering effects." *J. Geophys. Res.*, 80(23), 3322–3342.

Arroyo, M., Muir Wood, D., Greening, P. D., Medina, L., and Rio, J. (2006). "Effects of sample size on bender-based axial G_0 measurements." *Geotechnique*, 56(1), 39–52.

Cascante, G., and Santamarina, J. C. (1996). "Interparticle contact behavior and wave propagation." *J. Geotech. Engrg.*, 122(10), 831–839.

Campanella, R. G., and Vaid, Y. (1974). "Triaxial and plane strain creep rupture of an undisturbed clay." *Can. Geotech. J.*, 11(1), 1–10.

Gret, A. A. (2004). "Time-lapse monitoring with coda wave interferometry." Ph.D. thesis, Colorado School of Mines, Golden, CO.

Lee, J. S., and Santamarina, J. C. (2005). "Bender elements: Performance and signal interpretation." *J. Geotech. Geoenviron. Eng.*, 131(9), 1063–1070.

Mitchell, J. K., and Soga, K. (2005). *Fundamentals of soil behavior*, 3rd Ed., Wiley, Inc., New York.

Otheim, T. L., Adam, L., van Wijk, K., Batzle, M. L., McLing, T., and Podgorney, R. (2011). "CO_2 sequestration in basalt: Carbonate mineralization and fluid substitution." *The Leading Edge*, 30(12), 1354–1359.

Richart, F. E., Jr., Hall, J. R., and Woods, R. D. (1970). *Vibration of soils and foundations*, Prentice Hall, Englewood Cliffs, NJ.

Santamarina, J. C., and Fratta, D. (2005). *Discrete signals and inverse problems: An introduction for engineers and scientists*, Wiley, Chichester, U.K.

Santamarina, J. C., Klein, K. A., and Fam, M. A. (2001). *Soils and waves: Particulate materials behavior, characterization and process monitoring*, Wiley, Chichester, U.K.

Schurr, D. P., Kim, J. Y., Sabra, K. G., and Jacobs, L. J. (2011). "Damage detection in concrete using coda wave interferometry." *NDT Int.*, 44(8), 728–735.

Shapiro, N. M., Campillo, M., Stehly, L., and Ritzwoller, M. H. (2005). "High-resolution surface-wave tomography from ambient seismic noise." *Science*, 307(5715), 1615–1618.

Sens-Schönfelder, C., and Wegler, U. (2006). "Passive image interferometry and seasonal variations of seismic velocities at Merapi Volcano, Indonesia." *Geophys. Res. Lett.*, 33(21), L21302.

Singh, A., and Mitchell, J. K. (1968). "General stress-strain-time function for soils." *J. Soil Mech. and Found. Div.*, 94(1), 21–46.

Singh, A., and Mitchell, J. K. (1969). "Creep potential and creep rupture of soils." *Proc., 7th Int. Conf. on Soil Mechanics and Foundation Engineering*, Socieded Mexicana de Mecanica de Suelos, Mexico City, 379–384.

Snieder, R. (2006). "The theory of coda wave interferometry." *Pure Appl. Geophys.*, 163(2–3), 455–473.

Snieder, R., Grêt, A., Douma, H., and Scales, J. (2002). "Coda wave interferometry for estimating nonlinear behavior in seismic velocity." *Science*, 295(5563), 2253–2255.

Wuttke, F., Asslan, M., and Schanz, T. (2012). "Time-lapse monitoring of fabric changes in granular materials by coda wave interferometry." *J. ASTM Geotech Test.*, 35(2), 353–362.

Youn, J. U., Choo, Y. W., and Kim, D. S. (2008). "Measurement of small-strain shear modulus G_{max} of dry and saturated sands by bender element, resonant column, and torsional shear tests." *Can. Geotech. J.*, 45(10), 1426–1438.

J. Geotech. Geoenviron. Eng. 2013.139:1504-1511.